POLITECNICO DI MILANO

School of Industrial and Information Engineering

Department of Aerospace Science and Technology

SPACE PROPULSION

Final classwork report

Authors:
Niccolò BARDAZZI 10800456
Pietro GAZZI 10799381
Vincenzo PAOLELLA 10799255
Alvaro Sanchez VALVERDE 10753255
Christophe CHELLEMBROM 10758415
Enis ARIKAN 10775709
Alberto Castañeda SANCHEZ 10779073

29/05/2021
Academic Year 2020-2021

Contents

Abstract

A large amount of the current efforts of space propulsion research are concentrating into the development of increasingly smaller engines. Surely this tendency has became increasingly significant since the introduction of CUBESAT and NANOSAT standards and so one may relate this trend to the desire of decreasing the development costs of propulsion units. However, nowadays the environmental impacts of the propellants used in propulsion systems is becoming a very crucial aspect, and so far the architectures involving green propellants seem to work better at the small scales rather than the bigger ones. Hence, it seems that it is not just a matter of cost decreasing but there is also the desire to make the space propulsion a clean technology free from toxic propellants.
In this report, the feasibility analysis of a significantly small rocket electrolysis based engine is presented.

1 Technological framework and objectives definition

Given the reduced volume available in CubeSats, the main concern in terms of propulsion in this application nowadays is the research of Micro-thrusters. These thrusters are employed for station keeping, trajectory correction and compensation for gravitational perturbations [1]. Different technologies yield different ranges of thrust and specific impulse. A summary of the parameters of these technologies is found in Fig. 1.

System	Thrust	Specific Impulse	Technology Maturity
Electrospray	10-120μN	500-5000 s	TRL 6
Ion Engine	1-10 mN	1000-3500 s	TRL 4 (Iodine), TRL 8 (Xenon)
Hall Thruster	10-50 mN	1000-2000 s	TRL 4 (Iodine), TRL 8 (Xenon)
Non-toxic Thruster	0.1-27 N	220-250 s	TRL 6 (ADN-Ammonium dinitramide)
PPT, VAT	1-1300 μN	500-3000 s	TRL 8 (Teflon), TRL 7 (Titanium)
Hydrazine Thruster	0.5-4 N	150-250 s	TRL 6
Cold Gas Thruster	10 mN - 10 N	65-70 s	TRL 9 (Butane/$N_{2,gas}$)
Solar Sails	0.25-0.6 mN	—	TRL 6 (85m^2), TRL 7 (35) m^2

Figure 1: Propulsion Technologies [2]

Apart from the operational concerns, there are safety and economic concerns as well. There are restrictions related to the launch-vehicle safety, regarding for example the use of pressurized vessels and toxic propellants, for this reason non-hazardous propellants are going to be progressively more studied. The use of electrolysis propulsion systems seems, according to latest research, to fit well within these requirements and restrictions [3]. Electrolysis refers to the electro-chemical process by which water is converted into diatomic hydrogen and oxygen. By the use of water electrolysis, the following reaction is achieved [4].

$$H_2O_{(l)} + Power \rightarrow H_{2(g)} + 1/2O_{2(g)} \tag{1}$$

The products of this reaction can be effectively used as fuel (H_2) and oxidizer (O_2) in the combustion chamber of a CubeSat. Due to this, research effort has been spent on PEM electrolysis systems to provide propellant to such spacecrafts, obtaining the following benefits [5]:

- Water is a non-hazardous fluid, reducing the risk of explosion during the launch phase for the launcher and payloads. Furthermore, PEMs are able to operate in low power and are relatively cheap systems.
- Electric power needed for PEM can be easily generated by solar cells or secondary batteries. Furthermore, the propellant can be used as a battery, reducing mass requirements and eliminating electrical losses.
- The reaction involved in PEM produces exclusively H_2 and O_2 which may be used as fuel and oxidizer of a bi-propellant liquid engine. Moreover, it provides them in stoichiometric conditions, leading to a high flame temperature and producing as product of the combustion almost exclusively steam.

In the table 1 a collection of expected and measured performance of this kind of propulsion systems is reported. [5], [1].

It is worth to notice that electrolysis propulsion systems have not yet been flight proven except for the water based fuel cells which work in a very similar way to PEMs [1]. Actually a first demonstration of this technology has been launched in January 2021 by NASA in the PTD-1 mission. This mission still aims to prove the Hydros-C propulsion system, which is powered by solar arrays and uses a water electrolysis system [6].

Typical Electrolysis Propulsion System Parameters	
Parameter	**Value**
I_{sp}	300-350 s
Thrust	0.3-15 N
$\dot{m_{H_2}}$	1e-6 kg/s
$\dot{m_{O_2}}$	8e-6 kg/s
$P_{chamber}$	3 bar

Table 1: Parameters found in research

In light of what is presented above, this report aims to show the design and the optimization of a PEM based bi-propellant propulsion system for in-space application. The objectives of the analysis are:

- to design the propulsion unit in order to reach the highest total impulse
- to design the system's main components and to assess their manufacturing feasibility
- to assess the reliability and robustness of the system in an off-design condition.

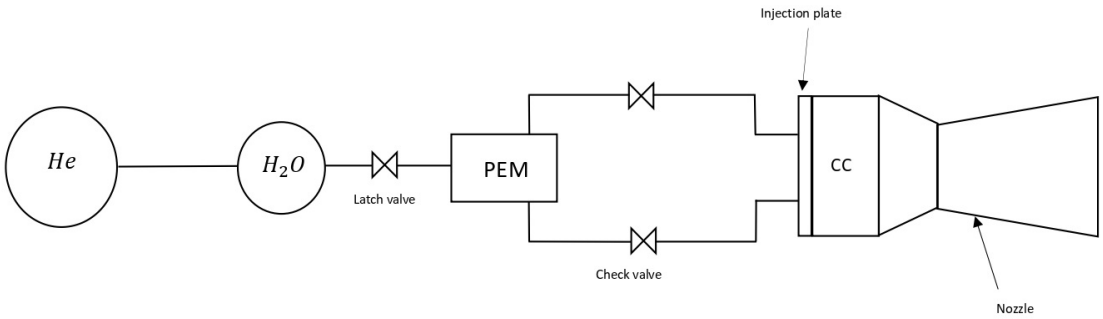

Figure 2: Engine scheme

2 Parametric ideal analysis

In this case of study, the PEM system is powered by an external source able to provide electric power which, in general, depends on the value of the pressure which the system operates at, as shown in the plot of Fig.3.

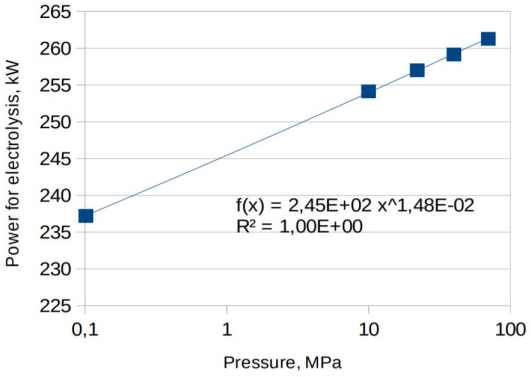

Figure 3: PEM:Electrolysis power (in kW) as a function of the output pressure for 1 mol/s water flow rate

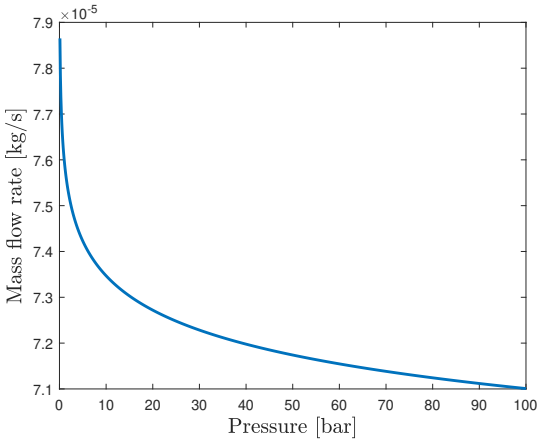

Figure 4: Mass flow rate elaborated with $1\,kW$

Given the analytical form reported in the plot, it has been possible to retrieve the mass flow rate of the system as a function of the pressure.
In the design of the engine, two types of requirements has been considered: the assignment requirements, reported in Table 2 typical for the specific application of a small satellite, and the technological requirements in Table 3.

Parameters	Values
Power	$1\,[kW]$
Mass	$0.5\,[kg]$
Max. D_{exit}	$30\,[mm]$

Table 2: External imposed requirements

Parameters	Values
Min. $D_t(800K)$	$0.074\,[mm]$
Min. $D_t(3200K)$	$0.588\,[mm]$
T_{cc}	$3210\,[K]$
ε	250
Application	CubeSat

Table 3: Structural/Technological requirements

Since this engine is designed to provide primary propulsion in vacuum conditions the expansion ratio ϵ has been assumed equal to 250, that is a common value for these kind of applications, e.g. in the case presented in [7] $\epsilon = 231$. The minimum diameter of the throat has been selected according to [8], that uses the Deep Reactive Ion Etching (DRIE) manufacturing technique for the nozzle production, while the maximum acceptable combustion chamber temperature has been imposed due to [5].

2.1 Procedure

Since the power for electrolysis is limited to 1 kW, water mass flow rate has been scaled linearly with respect to power so that if 1 mol/s requires 255 kW at 10 bar, 1 kW will produce only $\frac{1}{255}$ mol/s at the same pressure.
From Eq.1 it is clear that the PEM returns:

- 1 mol of H_2, $M_{H_2} = 2.01588$ g/mol,
- 1/2 mol of O_2, $M_{O_2} = 31.9988$ g/mol,

The dependency of mass flow rate on the water pressure is less appreciable. However, it slightly decreases with pressure increasing, keeping $\dot{m}_p$ in a range between 0.076 g/s at 1 bar and 0.071 g/s at 100 bar Fig. 4.
The system is not supposed to store neither hydrogen nor oxygen, hence all the fuel produced will

be consumed as soon it enters the propulsion unit. The combustion chamber (CC) analysis has been conducted with CEA software (NASA) with the Frozen Rocket model, that takes as input the pressure and computes M_{mol}, k, T_{CC}, v_t, ρ_t and μ_t. This computation has been performed for 20 values in a range between 1 and 100 bar. After that the results have been interpolated in order to evaluate the values at the remaining pressures. In Fig. 5 it has been displayed the results of the interpolation:

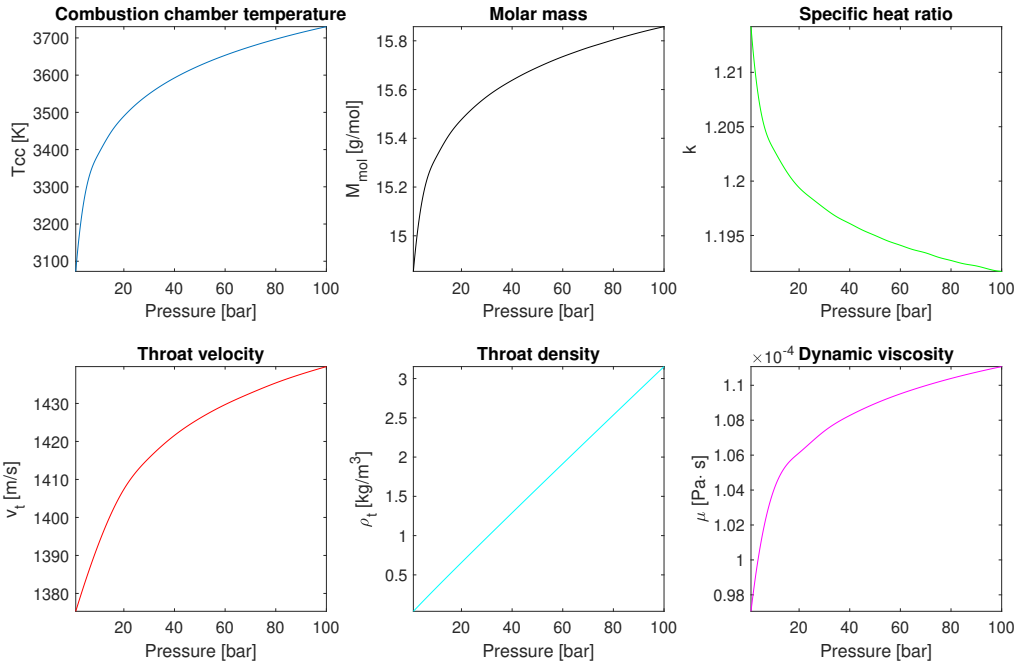

Figure 5: CEA results

Exploiting these results, it has been possible to compute the c* of the system using

$$c^* = \frac{1}{\Gamma(k)}\sqrt{\frac{\Re}{\mathcal{M}}T_c} \quad \text{where} \quad \Gamma(k) = \sqrt{k\frac{2}{k+1}^{\frac{k+1}{k-1}}}; \tag{2}$$

and then to retrieve the throat area A_t, considering as $\dot{m}_p$ the one elaborated by the PEM for the particular level of pressure p_c

$$A_t = \frac{c^*\dot{m}_p}{p_c} \tag{3}$$

Once the throat area has been computed, the ratio P_e/P_0 between the exit pressure of the nozzle and the pressure inside the CC can be recovered using the fsolve.m function in MATLAB for the Eq.4. Then Eq.5 has been applied achieving an ideal thrust coefficient (no nozzle losses).
6.

$$\frac{1}{\varepsilon} = \frac{A_t}{A_e} = \left(\frac{k+1}{2}\right)^{\frac{1}{k-1}}\left(\frac{P_e}{P_0}\right)^{\frac{1}{k}}\sqrt{\frac{k+1}{k-1}\left[1-\left(\frac{P_e}{P_0}\right)^{\frac{k-1}{k}}\right]} \tag{4}$$

$$c_{Tideal} = \sqrt{\frac{2k^2}{k-1}\left(\frac{2}{k+1}\right)^{k+1}\left[1-\left(\frac{P_e}{P_0}\right)^{\frac{k-1}{k}}\right]} + \left(\frac{P_e - P_a}{P_0}\right)\frac{A_e}{A_t} \tag{5}$$

Two of the main performance parameters of the engine are displayed in the following figure:

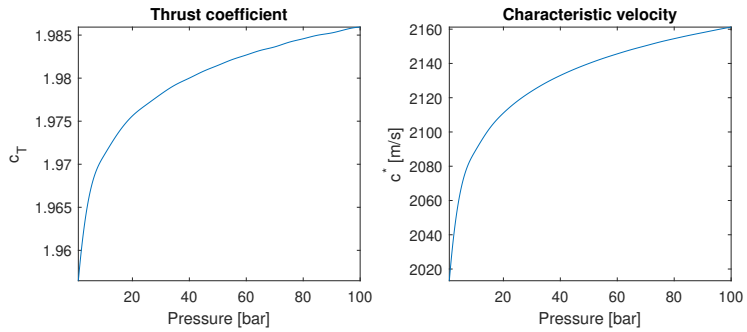

Figure 6: Parameters of merit

2.2 Results

At the end of the procedure described in previous section, it has been possible to compute the thrust, the specific impulse, the burning time and the total impulse:

$$I_{sp} = \frac{c_T c^*}{g_0} \qquad T = c_T \, A_t \, P_0 \tag{6}$$

$$t_b = \frac{m}{\dot{m}_p} \qquad I_{tot} = \int_0^{t_b} T \, dt \tag{7}$$

In order to compute the total impulse, the thrust has been assumed constant during the firing, thus the integral shown in Eq.7 simplifies in $I_{tot} = T \cdot t_b$, where T is the thrust and t_b is the burning time. In fig.7 the performance of the engine are presented and nozzle losses have been taken into account for all of them with particular attention to the thrust.

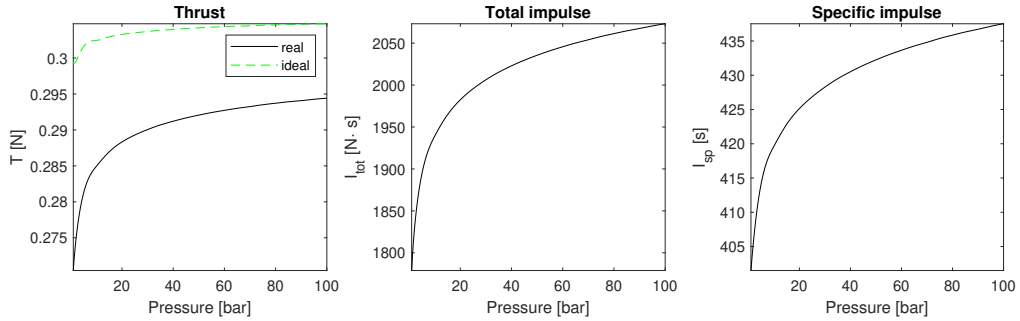

Figure 7: Engine performances

3 Optimization

3.1 Ideal optimization

It is clear from Fig. 7 that the optimization is a one way road: increasing the pressure means increasing all the performances. However, it should be considered that the higher the pressure, the higher the temperature in the CC and the lower the nozzle throat diameter. Therefore, during the design process of the engine the trade-off is between performances and structural/manufacturing feasibility of the system. From Table 3 the maximum achievable temperature T_{cc} is equal to 3280 K [5], while one of the smallest nozzle throat diameter for a bi-propellant electrolysis based system (O/F = 8, T = 3280 K) has been 0.0246 in (588 μm) [9].
In order to assess the best trade-off aimed to reach the highest total impulse for the engine presented in this case of study, it has been decided to perform a Pareto analysis taking in account all the constraints above described.

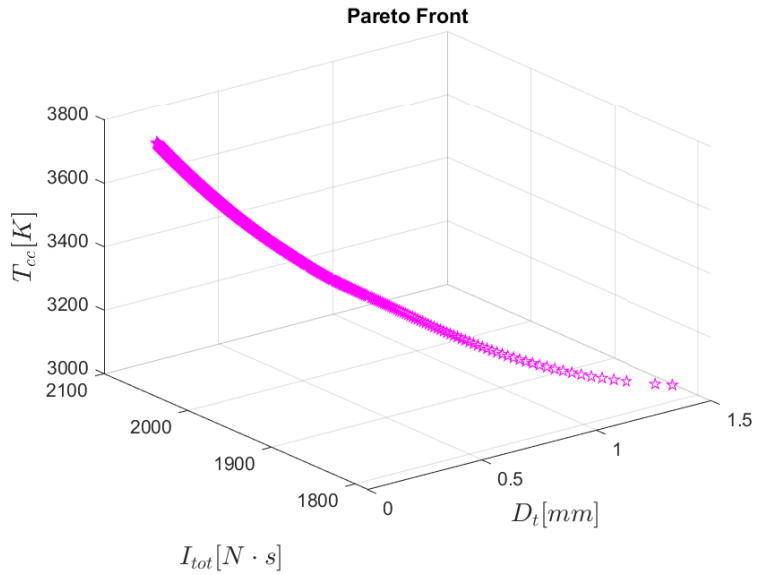

Figure 8: Pareto front with I_{tot}, T_{cc} and D_t as objectives

According to what is shown in Fig. 8, it is clear that the most strict constraint is the temperature, whereas the throat diameter fulfills in an easier way the technological requirement presented at Table 3. For the maximum achievable temperature, 3280 K, the nozzle throat diameter should be of 648 μm .

Parameters	Values
P_{cc}	4.65 $[bar]$
I_{sp}	412 $[s]$
T	0.2801 $[N]$
I_{tot}	1885 $[N\ s]$

Table 4: Optimal performances for the water engine motor

3.2 Iteration process

In the Sec.3.1 it has been shown how the maximum achievable CC pressure has been recovered. The next step of the design is the evaluation of the tank pressure and the losses along the line. These values have been obtained through an iterative analysis.
The iteration process has started by fixing the CC pressure to the ideal one previously derived and the velocity of fuel and oxidizer inside the injection plate according to Sec.4.1.1. This iteration aimed to find the value of the tank pressure P_t such that:

$$P_t = P_{CC} + \Delta P \tag{8}$$

Where the ΔP is a function of the mass flow rate Eq.9 that is function itself of the tank pressure Fig. 4. Pressure losses in the valves are neglected due to the much lower contribution with respect to the injection ones (see below Sec. 4.2.2) hence the ΔP has been considered equal to ΔP_{inj}.
As first step of the iteration, the pressure losses have been considered as a 25% of the P_{CC}. Then it has been used MATLAB's function fsolve.m, which identifies the P_t able to minimize the non-linear function $f(P_t) = P_t - P_{CC} - \Delta P(P_t)$ where P_{CC} is the one in Table 5. Once this parameter has been evaluated, the operating mass flow rate has been computed and all the sizing dimensions connected to its value can be retrieved.

3.3 Off-design

In this paragraph it is analyzed how the engine performs in off-design conditions, which are ±0.2 kW respect to the nominal condition. Hardware has been already fixed for the design conditions, thus the

workflow adopted follows the order of the engine components with no iterations since the latch valve and check valves have a negligible contribution as shown in Sec.4.2.2. Starting from the same P_t it has been evaluated the mass flow rate at different power level and the linked parameters.

Parameter	**Nominal**	+20 %	−20 %
$P_t\,[bar]$	5.64	5.64	5.64
$\dot{m}_p\,[g/s]$	0.074	0.089	0.059
$Power\,[kW]$	1	1.2	0.8
$P_{cc}\,[bar]$	4.65	4.22	5.00
$T_{cc}\,[K]$	3278	3262	3290
$\Delta P_{inj}\,[bar]$	0.99	1.41	0.63
C_d	0.9313	0.9281	0.9336
$I_{sp}\,[s]$	413	412	414
$T\,[N]$	0.2801	0.3333	0.2244
$I_{tot}\,[N\,s]$	1884	1874	1893

Table 5: Nominal and off-design parameters

As displayed in Table 5 more power is associated to more propellant mass flow rate thus the velocity will increase cause injectors' geometry has been fixed before. This leads to higher pressure losses in the injection hence lower pressure in the CC. When the CC reaction is at a lower pressure, the flame temperature will be lower as well. This means that the more dangerous off-design condition is the one with lower power because T_{cc} and P_{cc} reaches their maximum, 3290 K at 5 bar. Since it is an off-design condition it is expected to last as minimum as possible otherwise the engine could be compromised. Regarding the performances, the thrust increases when power provided is higher since the $\dot{m}_p$ grows, while the specific impulse slightly changes cause the static contribution in c_t increases but due to lower T_{cc}, c^* decreases. The last performance parameter, I_{tot} should have been kept constant, however in this case the Reynolds number (Re) is very low, therefore C_d plays a key role.

4 System design

4.1 Engine components design

In this section, the design of the main engine components has been shown. This does not include also the design of the Polymer Electrolyte Membrane but only the one concerning the part of the engine after the two final check valves.

4.1.1 Injection head

The injection head has been designed with one to one fuel and oxidizer configuration due to restrictions imposed by the CC cross sectional area and in order to minimize the losses as shown in Eq. 9. Firstly it has been decided an inlet velocity of the flow of 35 m/s at nominal condition, then verified that the Mach number was such that the flow could be considered incompressible ($M < 0.3$), even in off-design. At the end, losses are computed along the injection plate with the trade-off with respect to the dimension of the injection area:

$$\Delta P_{inj} = \frac{8}{\rho}\left(\frac{\dot{m}}{A_{inj}C_d}\right)^2 \tag{9}$$

where C_d is the discharge coefficient dependent only on the geometry [10]. It has been imposed the same losses both for O_2 and H_2 lines hence once $C_d(O_2)$ has been fixed while $C_d(H_2)$ can be recovered. $C_d(O_2) = 0.85$ and $C_d(H_2) = 0.21$.

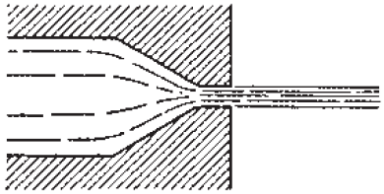

Figure 9: Injector shape O_2

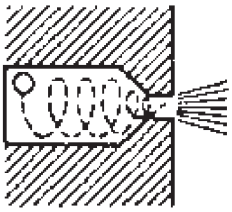

Figure 10: Injector shape H_2

Type	Diameter [mm]	Discharge coeff
Short with conical	0.574	0.85
Short with spiral	0.811	0.21

Figure 11: Discharge Coefficient [10]

Another factor to be chosen has been β, that is the ratio between the hole diameter and the pipe diameter, for which a typical value is 0.25 [11], as used in most of orifice plate installations. In this way the pipe diameter is fixed therefore the valve can be designed from this point on as it has been done in Sec.4.2.2.

4.1.2 Combustion chamber

In order to design the combustion chamber, the first thing selected has been the proper characteristic length L* to grant the right residence time for the reactants. For this case of study, a propellant made of H_2 and O_2 in gaseous state, it has been chosen an $L^* = 0.71$ m, which is the highest value of the range proposed in [12] selected to be conservative. Even though this value was for LO_2/GH_2 it has been assumed to be valid also for GO_2/GH_2.
The Mach number in throat must arrive to the sonic condition $M_y = 1$ starting from M_x which has been selected to 0.025 in order to reach a proper L/D ratio as seen in [5]. Using the following equation:

$$\frac{1}{\varepsilon_c} = \frac{A_y}{A_x} = \frac{M_x}{M_y}\sqrt{\left\{\frac{1+[\frac{k-1}{2}]M_y^2}{1+[\frac{k-1}{2}]M_x^2}\right\}^{\frac{k+1}{k-1}}} \tag{10}$$

it has been possible to find the contraction coefficient ε_c and, according to $D_t = 0.648\ mm$ (found in Sec.4.1.3), the length and volume of CC have been computed:

$$V_c = A_t L^* \quad \text{and} \quad L = \frac{L^*}{\varepsilon_c} \tag{11}$$

The numerical outcomes of the above described design process are:

Parameter	Value
V_c	234 $[mm^3]$
L_c	7.2012 $[mm]$
d_c	6.4333 $[mm]$
ε_c	98.5950

Table 6: Combustion Chamber Design

The final products of the CC reaction have been computed through the CEA software, Eq. 12, showing high dissociation before the nozzle inlet.

$$H_2 + \frac{1}{2}O_2 \rightarrow 0.611H_2O + 0.113OH + 0.060H + 0.044O_2 + 0.142H_2 + 0.026O \tag{12}$$

4.1.3 Nozzle

To complete the design of the engine, the attention was then turned to the nozzle, which was chosen to be conical due to its manufacturing simplicity. The divergence angle α and the convergence angle β have been assumed to be 15°and 45°[10], therefore the divergent and convergence part of the nozzle are:

$$L_c = \frac{r_e - r_t}{tan(\alpha)} \quad \text{and} \quad L_d = \frac{r_{cc} - r_t}{tan(\beta)} \tag{13}$$

Due to the fact that the conical nozzle's exit walls are not parallel to the exiting flow, there is inevitably some losses regarding the radial exit velocity. With the use of the divergence angle, the divergence loss factor was then computed:

$$\lambda = \frac{1 + cos(\alpha)}{2} \tag{14}$$

A divergence factor of 0.9830 is obtained as constant value with pressure as shown in Fig. 12. This value can be directly correlated to the I_{sp}, where a loss of 1.7 % is generated due to the shape of the nozzle. In addition, since this nozzle is in the micro-propulsion field we expect a significantly reduced value of the mass flow rate. For this reason the discharge coefficient C_d, defined as the ratio between the real mass flow rate at the throat area with respect to the ideal one, has been computed according to Eq.15 and has been shown as function of the PEM pressure in Fig.12.

$$C_D = 1 - \left(\frac{\gamma+1}{2}\right)^{0.75}\left(3.266 - \frac{2.128}{\gamma+1}\right) Re'^{-0.5} + 0.9428\frac{(\gamma-1)(\gamma+2)}{(\gamma+1)^{0.5}} Re'^{-1} \tag{15}$$

For technological reason it has been decided to assign a ratio between the curvature at the throat with respect to the throat radius of 1.2 to recover the modified Re, Re':

$$Re' = \sqrt{\frac{r_t}{r_c}} Re_t \quad where \quad Re_t = \frac{\rho_t v_t d_t}{\mu_t} \tag{16}$$

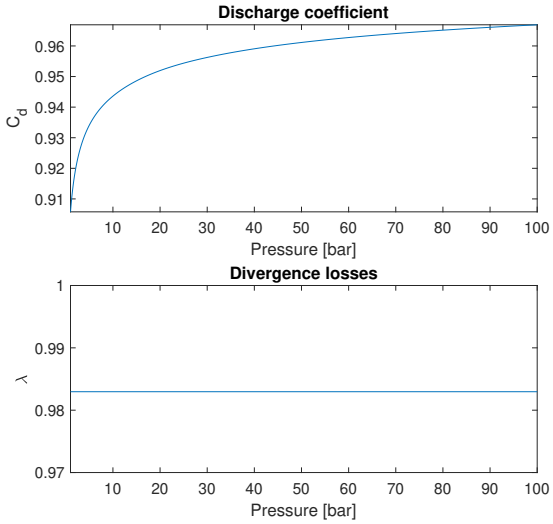

Figure 12: Discharge coefficient and divergence loss coefficient

Parameters	Values
$\mathbf{d_t}$	0.650 $[mm]$
$\mathbf{d_e}$	10.2 $[mm]$
$\mathbf{L}$	20.8 $[mm]$

Table 7: Nozzle parameters

In this particular application $Re = 1287.5$ leading to a $C_d = 0.9313$, which is a typical value for micro-propulsion systems.

4.2 Water supply system

In this section the design process of water supply system is reported. This is a pressurized system so it relies on a tank of gas, helium in this case, to keep the pressure of fuel at the right level in order to have a correctly working engine.

4.2.1 Tanks

The design has started from an assumption on the shape of the two tanks, indeed they have been supposed to have a spherical geometry. From the mass of water and its density, it has been possible to know the total volume which has been increased of 2% to overcome unexpected losses. Given the assumption on the shape tanks, the respective radius has been easily computed using,

$$r = \sqrt[3]{\frac{3V}{4\pi}} \tag{17}$$

The pressure value of the water tank p_{H_2O} has affected the design of both vessels. Their thicknesses have been found by means of:

$$t = \frac{p_b r}{2\sigma_{ut}} \tag{18}$$

where σ_{ut} is the ultimate tensile strength of the tank material and p_b is the burst pressure assumed to be twice the internal pressure of the fluid.
Regarding the pressurant gas, it has been assumed that the expansion process was an isentropic transformation and so during it, the gas temperature would decrease while the volume would do the opposite. Hence, once the water was totally expelled, the pressurant gas would occupy both the water tank and the one of helium. From this the initial volume of helium tank has been computed using:

$$V_{He,f} = \frac{V_{H_2O}}{1 - \frac{p_{He,f}}{p_{He,i}} \frac{T_{He,i}}{T_{He,f}}} \tag{19}$$

$$V_{He,i} = V_{He,f} - V_{H_2O} \tag{20}$$

Finally, using Eq. 17 and 18 the thickness of helium tank has been derived. During the design process, four materials have been used (Aluminum alloy 2219, Titanium, Steel 4130, Graphite carbon fiber) and the results obtained are the following:

Material	$t_{He}\,[mm]$	$M_{He}\,[g]$	$t_{H_2O}\,[mm]$	$M_{H_2O}\,[g]$
Steel	0.091	50.88	0.032	7.859
Aluminium	0.367	73.30	0.131	11.32
Titanium	0.064	20.31	0.022	3.13
Graphite composite	0.088	9.70	0.031	1.49

Table 8: Water and helium tanks design

The tank has been sized to store helium with an initial pressure of 6.22 bar till 5.64 bar at the end of the mission. The helium has been stored at 310 K since for safety reason it should be kept above water freezing point but also under water boiling point. In light of the values shown above, it seems reasonable from a technological as well as a performance point of view, to choose the aluminum as material for the construction of the two tanks. However, a more feasible thickness for them, considering the usual thickness of the foils present in commerce, should be considered such as 0.5 mm. With this design choice the final mass of two tanks would be $M_{He} = 280$g and $M_{H_2O} = 43$g.

4.2.2 Valves

As shown in Fig. 2, the water flow has to go through a latch valve and, after the PEM, the H_2 and O_2 flows go through a check valve each. At the beginning of the design process of the valves, some constraints concerning the feed lines have been took in account:

- Speed of injection downstream fluids: 35 m/s
- β parameter of injection head: 0.25
- Water speed out of the tank 2.4 mm/s
- Water mass flow rate: $7.4{\cdot}10^{-5}$ kg/s

Considering what just reported and the ideal optimal pressure of water tank $P = 5.64$ bar, it was found that the feed lines were characterized by:

- Diameter water pipe: 6.4 mm
- Diameter H_2 pipe: 3.2 mm
- Diameter O_2 pipe: 2.3 mm

From an initial literature research of commercial valves for space applications (Appendix A), it has been possible to select some of them feasible for this case of study. For the computation of the actual system performance, it has been necessary to calculate the pressure losses through the valves and, in order to do so, the following relation has been employed:

$$\Delta P = \frac{SG * Q^2}{Cv^2} \tag{21}$$

where ΔP is the pressure loss in psi, SG is the density ratio of the fluid to the density of water, Q is the volumetric flow rate in gallons per minute (gpm) and Cv is the flow coefficient of the valve.

Latch valve

The valve needed is similar to the latch valve offered by the Ariane Group (A1 - Fig. 15). This one is compatible with water, it can work up to 20 g/s, which is larger than the flow rate of 0.074 g/s of the system, it works up to 25 bar and has an inlet diameter equal to that of the water pipe, 6.35 mm. From the data-sheet [13], knowing that at 4.5 g/s there was a 0.15 bar loss, a Cv of 0.05 was found out by means of Eq. 21. Using that Cv and the volume flow rate of the water line, the pressure loss obtained has been 0.04 millibar. This latter could be considered almost negligible when compared to the operational pressure of the engine.

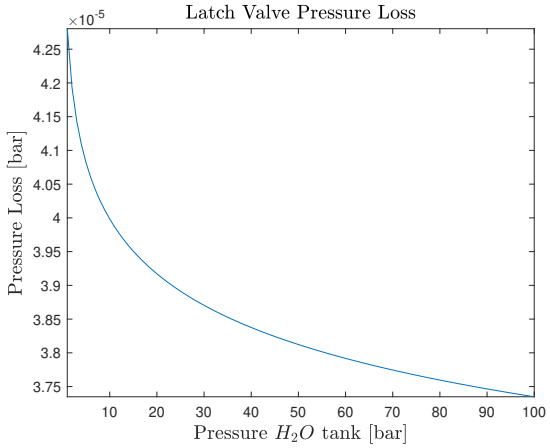

Figure 13: Pressure losses of latch valve varying the pressure of H_2O tank

Check valves

The valve needed is similar to the Circor Aerospace 1PP valve (A1- Fig. 18). This valve is compatible with gases and has a diameter of 3.17 - 5 mm. In order to compute the valve's Cv, the graph in Fig. 18 which correlates flow rate to ΔP has been used. Referring to the 1PP valve curve for air and taking the point of 10 scfm and 4 psi, the Cv computed has been 1.31. Using that Cv of the valve and the Q of O_2 and H_2 lines, the pressure losses obtained were 0.006 millibar and 0.002 millibar respectively. It was noted that the pressure losses through the two different valves had to be the same, in order to let the flows enter with the same pressure into the combustion chamber. To do that the valves would have had different Cv however, as the pressure losses were almost negligible with respect to the operating pressure, for this stage of development, it was assumed that the same valve could be used.

It is worth to precise that experimental verification shall be conducted on the valves to accurately determine their Cv and the pressure loss as flow rate varying. Moreover, due to the fact that some technical information is missing from the data-sheets, and the diameters of the system pipes are not exactly the same as the inlet diameters of the valves, the following requirements apply for the manufacturer:

- O_2

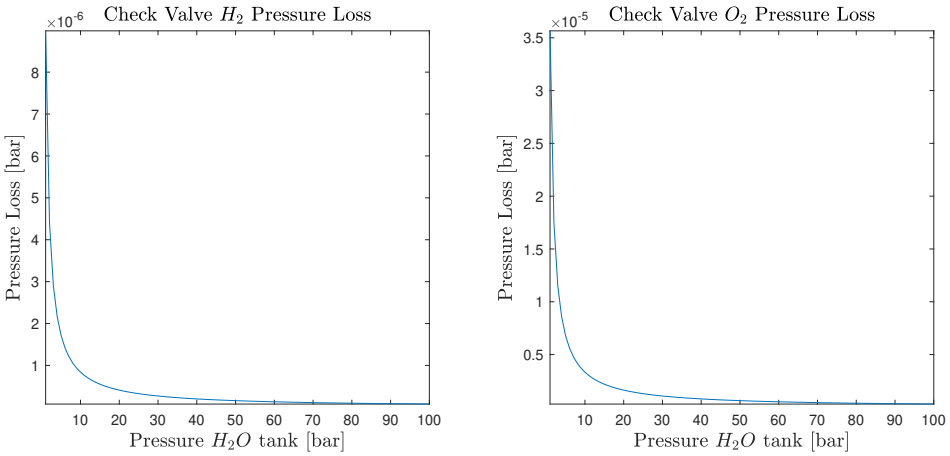

Figure 14: Pressure losses of check valves varying the pressure of H_2O tank

  - The check valve shall be plugged into a pipe of 2.3 mm diameter
  - The check valve shall be able to work with a mass flow rate of 0.07 g/s
  - The check valve shall have a Cv of 1.31

- H_2
  - The check valve shall be plugged into a pipe of 3.2 mm diameter
  - The check valve shall be able to work with a mass flow rate of 0.0083 g/s
  - The check valve shall have a Cv of 1.31

- **General**
  - Some tolerance might be considered for the Cv of both valves as long as both provide a similar pressure drop for the specific O_2 and H_2 flow and this pressure loss is less than 0.1 millibar

5 Conclusions

CubeSats are a promising field of application in the space industry, due to their low mass and cost, although up to now their application has been limited to almost passive systems. The possibility to introduce a primary micro-propulsion unit is a crucial aspect in this research field. The priliminary analysis conducted above reveals that a PEM based engine can fulfil the requirements of this kind of application, in fact the I_{sp} reaches values higher than 400 s, with a 300 mN thrust . These performances are possible thanks to the reaction between H_2 and O_2 that is one of the most efficient fuel-oxidizer couple, with almost non-existent environmental issues, the chemical point of view cannot pushed further. The construction constraints are the most relevant limitation of this engine, a further work should analyze deeper the effect of high temperature and pressure to the micro-size combustion chamber, starting with 3D CFD analysis and then with real experiments, investigating also new manufacturing techniques. From this preliminary analysis we can underline two possible strategies in order to improve the engine. Since the performances increase at higher combustion pressure, a possible refinement version could be achieved providing the CC an efficient cooling system able to keep the temperature values below the dangerous ones. Another improvement could be a better design of the nozzle, that has been modelled with conical shape, due to its construction simplicity, but that can be replaced by a bell-shaped one, that returns better performances but an higher attention related to the production process.

References

[1] J. A. e. a. Popescu, *Experimental approach regarding the ignition of H2/O2 mixtures in vacuum environment.* CEAS 2017, 16-20, 2017.

[2] C. J. e. a. Pascoa, *A preview of propulsion systems for cubesats.* ASME, 2018.

[3] R. A. Zeledon, *electrolysis propulsion for small-scale spacecraft.* Cornell University, 2015.

[4] M. Carmo, *A comprehensive review on PEM water electrolysis.* Elsevier Ltd., 2013.

[5] A. Minotti, "A new nanosats propulsion system: swirling-combustion chamber and water electrolysis," *AIMS Energy*, vol. 6, no. 3, pp. 402–413, 2018.

[6] NASA, "Demonstrating novel cubesat technologies in low-earth orbit"."

[7] A. London, A. Epstein, and J. Kerrebrock, "High-pressure bipropellant microrocket engine," *Journal of Propulsion and Power*, vol. 17, no. 4, pp. 780–787, 2001.

[8] M. C. Louwerse, H. V. Jansen, M. N. W. Groenendijk, and M. C. Elwenspoek, "Nozzle fabrication for micropropulsion of a microsatellite," *Journal of Micromechanics and Microengineering*, vol. 19, p. 045008, mar 2009.

[9] Y. J. M. Liu, "Performance testing of various nozzle designs for water electrolysis thruster," in *54th AIAA Aerospace Sciences Meeting*, p. 0954, 2016.

[10] G. P. Sutton and O. Biblarz, *Rocket propulsion elements.* John Wiley & Sons, 2016.

[11] Chemical Engineering Now, "Orifice Sizing Principles." `http://chemicalengineeringnow.com/OrificesPrinciples.htm`. Accessed: 2021-05-29.

[12] G. Henry, R. Humble, W. Larson, U. S. D. of Defense, U. S. N. Aeronautics, and S. Administration, *Space Propulsion Analysis and Design.* College custom series, McGraw-Hill, 1995.

[13] Ariane Group, "Latch valves for space propulsion systems." `https://www.space-propulsion.com/brochures/valves/space-propulsion-valves.pdf`. Accessed: 2021-05-29.

[14] MAROTTA, "Latch valve model MV602L." `https://marotta.com/products/flow-controls/satellite-propulsion-controls/miniature-solenoid-valves/`. Accessed: 2021-05-29.

[15] T. S. Technologies, "Latch valve model TS-160T." `https://www.triton-space.com/ts-160s`. Accessed: 2021-05-29.

[16] CIRCOR Aerospace, "Check valve 200 series." `https://circoraerospace.com/downloads/cai/fluidcontrols/pdf/200\%20Series\%20CV2.pdf`. Accessed: 2021-05-29.

[17] Staiger, "Micro valve model VA 204-715." `https://www.staiger.de/en-us/products/online-catalogue/details?name=VA20204-715`. Accessed: 2021-05-29.

Appendices

A Commercial valves

A.1 Latch valves

Searching with several suppliers that have products used in the aerospace industry, the following candidates were found.

Latch Valve Technical Characteristics	
Characteristics	**Nominal Value**
Tubing Interface	1/4 inch
Mass	545 g
Operating voltage	22-32 VDC
Response time	< 30 ms
Coil resistance	37,5 Ω ± 1,5 Ω
Max.operating pressure	24,25 bar
Back-Relief Pressure	8 to 14 bar
Flow Rate and Pressure Drop	< 0.15 bar at 4.5 g/s
Fluid Compatibility	Water, hydrazine, MMH, NTO, IPA, He, N_2, Xe and others

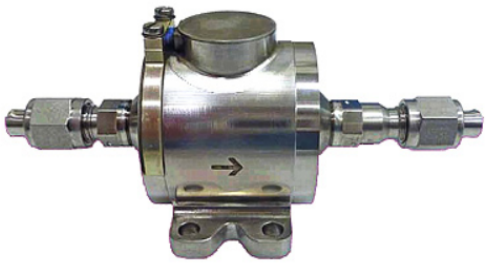

Figure 15: Ariane Group Latch valve [13]

PARAMETER	MV602L
Inlet Pressure	2900 psi (200 Bar)
Proof	4350 psi (300 Bar)
Burst	7240 psi (500 Bar)
Operating Temperature	- 13°F to 122°F (- 25°C to 50°C)
Non-Operating Temperature	- 22°F to 122°F (- 30°C to 50°C)
Internal Leakage	<1 x 10-4 sccs GHe
External Leakage	≤1 x 10-6 sccs GHe
Flow Capacity	ESEOD 0.014" Cd = 0.6

Figure 16: MAROTTA MV602L valve [14]

Valve Specifications	TS-160S
Pressure Range	100-3,000 psig
Proof Pressure	4,500 psig
Burst Pressure	7,500 psig
Electrical Connector	MIL-DTL-38999/25YA98PN
Operating Voltage	28VDC
Liquid Flow Coefficient (Cv)	13
ESEOD	0.85 in
Body Material	Aluminum (7075-T651) Stainless Steel (17-4)
Fasteners	Stainless Steel (A286)
Operating Temperature	-65°F to 150°F

Figure 17: Triton Space Technologies model TS-160T valve [15]

A.2 Check valves

PP — FEMALE PIPE

Dash No.	Pipe Size	A	C Hex.&Rd.	D	Weights (lbs.) Alum.	Brass	All Steel
1PP	1/8"	1.70	.81	.62	.05	.15	.14
2PP	1/4"	2.25	1.00	.75	.12	.36	.34
3PP	3/8"	2.43	1.12	.88	.15	.46	.43
4PP	1/2"	2.93	1.50	1.25	.32	.98	.92
6PP	3/4"	3.37	1.75	1.50	.49	1.50	1.41
8PP	1"	3.99	2.00	1.75	.73	2.25	2.11
10PP	1-1/4"	4.50	2.75	2.25	1.60	5.00	4.80
12PP	1-1/2"	5.35	2.75	2.25	1.73	5.34	4.97
16PP	2"	6.10	3.50	2.75	2.60	8.00	7.50

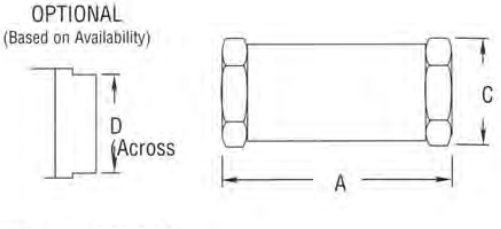

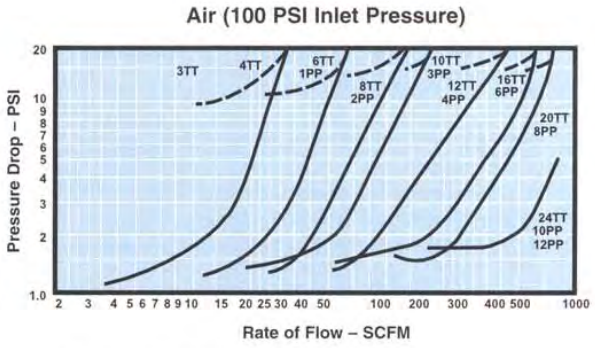

Figure 18: CIRCOR Aerospace 200 series 1PP valve [16]

VA 204-7

2/2-Wege-Magnetventil
direktgesteuert, NC
(stromlos geschlossen)

Anwendung
Neutrale und leicht aggressive Flüssigkeiten, Gase und Dämpfe

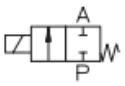

Typ/ Best.-Nr.	Baugröße s [mm]	Nennweite [mm]	Anschluss	Druckdifferenz [bar]	kv-Wert [m³/h]	Gewicht [kg]
VA 204-715	7	0,3	Cartridge	0 - 10	---	0,003
Dichtwerkstoff:	**P** (NBR)	**E** (EPDM)	**V** (FPM)	**Z** (FFKM)		

Gehäusewerkstoff:	Edelstahl (1.4305)	Leistungsaufnahme:	0,5 - 1 W
Innenteile:	Edelstahl (1.4310/1.4105)	Zul. Spannungstoleranz:	-15 %... +10 %
Einbaulage:	beliebig, bevorzugt steh.	Rel. Einschaltdauer (ED):	100 %
Max. Umgebungstemp.:	50 °C	Schalthäufigkeit:	max. 500 /s
Viskosität des Mediums:	max. 21 mm²/s (3 °E)	Schaltzeit:	0,5 ms bis 4 ms
Statischer Druck:	max. 20 bar		
Standardspannungen:	DC: 24 V, 12 V, 9 V, 6 V		

Figure 19: Staiger model VA 204 - 715 micro valve [17]